

A LINEAR ADAPTIVE SECOND-ORDER BACKWARD DIFFERENTIATION FORMULATION SCHEME FOR THE PHASE FIELD CRYSTAL EQUATION*

DIANMING HOU¹ ZHONGHUA QIAO²

ABSTRACT. In this paper, we present and analyze a linear fully discrete second order scheme with variable time steps for the phase field crystal equation. More precisely, we construct a linear adaptive time stepping scheme based on the second order backward differentiation formulation (BDF2) and use the Fourier spectral method for the spatial discretization. The scalar auxiliary variable approach is employed to deal with the nonlinear term, in which we only adopt a first order method to approximate the auxiliary variable. This treatment is extremely important in the derivation of the unconditional energy stability of the proposed adaptive BDF2 scheme. However, we find for the first time that this strategy will not affect the second order accuracy of the unknown phase function ϕ^n by setting the positive constant C_0 large enough such that $C_0 \geq 1/\tau$. The energy stability of the adaptive BDF2 scheme is established with a mild constraint on the adjacent time step ratio $\gamma_{n+1} := \tau_{n+1}/\tau_n \leq 4.8645$. Furthermore, a rigorous error estimate of the second order accuracy of ϕ^n is derived for the proposed scheme on the nonuniform mesh by using the uniform H^2 bound of the numerical solutions. Finally, some numerical experiments are carried out to validate the theoretical results and demonstrate the efficiency of the fully discrete adaptive BDF2 scheme.

1. INTRODUCTION

The phase field crystal (PFC) model was firstly proposed in [5, 6] and has been frequently used for modelling the crystal growth at the atomic scale in space but on diffusive scale in time. It can simulate nucleated crystallites at arbitrary locations and orientations with the elastic and plastic deformations. The PFC model can account for incorporating the periodic nature of the crystal

Date: May 30, 2023.

2020 Mathematics Subject Classification. 35K55, 65M12, 65M15, 65F30.

Key words and phrases. Phase field crystal equation, linear adaptive BDF2 scheme, scalar auxiliary variable approach, unconditional energy stability, convergence analysis.

*The work of D. Hou is supported by NSFC grant 12001248, the NSF of the Jiangsu Province grant BK20201020, the NSF of Universities in Jiangsu Province of China grant 20KJB110013 and the Hong Kong Polytechnic University grant 1-W00D. Z. Qiao's work is partially supported by the Hong Kong Research Grant Council RFS grant RFS2021-5S03 and GRF grant 15302919, the Hong Kong Polytechnic University internal grant 4-ZZLS, and the CAS AMSS-PolyU Joint Laboratory of Applied Mathematics.

¹School of Mathematics and Statistics, Jiangsu Normal University, 221116 Xuzhou, China. Current address: Department of Applied Mathematics, The Hong Kong Polytechnic University, Hung Hom, Kowloon, Hong Kong. (dmhou@stu.xmu.edu.cn).

²Corresponding author. Department of Applied Mathematics, The Hong Kong Polytechnic University, Hung Hom, Kowloon, Hong Kong. (zqiao@polyu.edu.hk).

lattices through the following Swift-Hohenberg type free energy, defined by

$$E(\phi) = \int_{\Omega} \left(\frac{1}{2} \phi (\Delta + \beta)^2 \phi + \frac{1}{4} \phi^4 - \frac{\varepsilon}{2} \phi^2 \right) d\mathbf{x}, \quad (1.1)$$

which is minimized by periodic density fields. Here $\Omega \subset \mathbb{R}^d, d = 2$ or 3 , ϕ is the atom density field, β and ε are two positive constants such that $0 < \varepsilon < \beta^2$. The operator $(\beta + \Delta)^2 \phi$ is defined by $(\Delta + \beta)^2 \phi = \Delta^2 \phi + 2\beta \Delta \phi + \beta^2 \phi$. Thus the conserved phase field crystal equation reads

$$\begin{cases} \frac{\partial \phi}{\partial t} = \Delta \mu, & \text{in } \Omega \times (0, T), \\ \mu = (\Delta + \beta)^2 \phi + \phi^3 - \varepsilon \phi, & \text{in } \Omega \times (0, T), \\ \phi(\mathbf{x}, 0) = \phi_0(\mathbf{x}), & \text{in } \Omega. \end{cases} \quad (1.2)$$

Due to the gradient structure of (1.2), the above PFC system satisfies the following energy dissipation law

$$\frac{d}{dt} E(\phi) = -\|\nabla \mu\|^2 \leq 0. \quad (1.3)$$

This indicates the free energy $E(\phi)$ always decreases in time. In numerical simulations, it is crucial to design numerical schemes preserving the above energy dissipation law at the discrete level, see e.g., [1, 7, 8, 10, 4, 30, 34, 26, 27, 18, 17, 22] and references therein. These schemes are often called energy stable schemes in practice. A direct implicit/explicit treatment for the nonlinear term in (1.2) usually yields a severe stability restriction on the time step sizes to preserve the discrete form of the energy law (1.3). In the last two decades, many efforts have been made to relax this restriction. For example, Wise, Wang and Lowengrub developed a first order convex splitting scheme for the PFC equation in [29]. The unconditional energy stability and the corresponding error estimate of their proposed scheme were rigorously established. The second order convex splitting method for the PFC model based on the Crank-Nicolson formula was also studied in their subsequent work [16]. They have proved that the Crank-Nicolson convex splitting scheme was unconditionally energy stable in the sense of the discrete free energy bounded by the initial one, which indicates the uniform L^∞ bound of the numerical solutions. Then the corresponding error estimate of the proposed scheme could be easily derived with the help of the uniform bound of the numerical solutions, seeing [3]. In [11], Guo and Xu presented first order and second order unconditionally energy stable schemes based on a local discontinuous Galerkin method with the convex splitting approach. An unconditionally energy stable BDF2 convex splitting scheme has been developed for the PFC model by Li, Mei and You in [19]. They rigorously established the mass conservation, the unconditional energy stability and the convergence of the proposed numerical scheme. Though all the above convex splitting schemes are uniquely solvable due to the gradient of a strictly convex function, their resulted nonlinear systems must be solved at each time step, which is relatively time-consuming. Thus it is highly desired to develop linear high order energy stable schemes for the PFC model (1.2). In [31], Yang et al. proposed two linear second order unconditionally energy stable schemes for the PFC equation using the invariant energy quadratization (IEQ) approach. Recently, Li and Shen have adopted the scalar auxiliary variable (SAV) approach to construct a linear Crank-Nicolson scheme for the PFC model in [20], where the unconditional energy stability and the corresponding error estimate of the fully discrete scheme were rigorously proved.

Another important feature of the PFC model is that its evolution process usually takes rather long time before it reaches the steady state. Moreover, in this process, the solution of the PFC equation usually undergoes both fast and slow changes at different time. Therefore, it is reasonable to employ some time adaptive strategies in the simulation, where unconditionally energy stable numerical schemes with variable time steps are very needed. Combining the second order Crank-Nicolson convex splitting scheme, an adaptive time-stepping strategy based on the variation of the free energy was adopted for the PFC model in [33], where both the steady-state solution and the dynamical changes of the solution have been resolved accurately and efficiently. As known, the BDF2 schemes usually achieve stronger stability than the one based on the Crank-Nicolson formula, especially for the equations with strong stiffness [12, 14, 32]. Recently, an adaptive fully implicit BDF2 time-stepping method was studied for the PFC model in [21]. Under a restriction on the adjacent time-step ratio $\gamma_n \leq 3.561$, the energy stability and the corresponding L^2 error estimate of the proposed adaptive scheme were rigorously derived by using the discrete orthogonal convolution kernels and convolution inequalities. However, these adaptive time-stepping schemes in [21, 33] are also nonlinear and the nonlinear iteration is unavoidable at each time step. Very recently, combining the nonuniform BDF2 formula and the SAV approach, we successfully derived a linear second order unconditionally energy stable time stepping scheme for gradient flows with the adjacent time-step ratio $\gamma_n \leq 4.8465$ in [13]. Though it avoids solving the nonlinear system for the phase function ϕ^n by explicit treatment for the nonlinear term, there still exists a nonlinear algebraic equation to be solved for the auxiliary variable at each time step.

The goal of this paper is to develop and analyze a linear second order adaptive time-stepping scheme based on the BDF2 formula for the PFC model (1.2) using the SAV approach proposed in [26, 27]. The linear BDF2 scheme based on the SAV approach has been proved unconditionally energy stable on the uniform temporal mesh for the PFC model in [31]. However, it seems to be rather difficult to prove similar results on nonuniform temporal meshes. In this paper, we construct a linear unconditionally energy stable BDF2 scheme for the PFC model on the nonuniform temporal mesh for the first time by using a first order approximation on the auxiliary variable. The first order treatment of the auxiliary variable will not affect the second order accuracy of the unknown atom density field ϕ^n by setting the positive constant C_0 large enough such that $C_0 \geq 1/\tau$. Moreover, the constructed adaptive BDF2 scheme avoids solving the nonlinear algebraic equation for the auxiliary variable as needed in our previous work [13]. More precisely, there are only two sixth-order equations with constant coefficients to be solved at each time step, which can be solved efficiently by exiting fast Poisson solvers. Furthermore, under a mild restriction on the adjacent time-step ratio $\gamma_n \leq 4.8465$, we rigorously establish the unconditional energy stability and the corresponding error estimate of the proposed fully discrete BDF2 scheme on the nonuniform temporal mesh.

The rest of the paper is organized as follows. In section 2, we review the SAV method proposed in [26, 27], and construct the linear BDF2 scheme on the nonuniform temporal mesh. The unconditional energy stability for the proposed scheme is rigorously proved in the sense of a modified discrete energy. In section 3, a rigorous error estimate of the fully discrete adaptive BDF2 scheme is derived for the PFC model, which shows the second order accuracy of the numerical solution ϕ^n in time with larger enough constant C_0 such that $C_0 \geq 1/\tau$. Several

numerical examples are given in section 4 to validate the theoretical results and the efficiency of the proposed method. Finally, the paper ends with some concluding remarks in section 5.

2. SCALAR AUXILIARY VARIABLE APPROACH

We first introduce some notations which will be used throughout the paper. Denote $\|\cdot\|_m$ the standard H^m norm. The norm and inner product of $L^2(\Omega) := H^0(\Omega)$ are denoted by $\|\cdot\|$ and (\cdot, \cdot) , respectively. For the sake of simplicity, we consider the periodic boundary condition for (1.2).

The key idea of the SAV approach [12, 26] is to transform the nonlinear term to a simple quadratic form by introducing a scalar auxiliary variable $r(t)$, defined by

$$r(t) = \sqrt{E_1(\phi) + C_0} := \sqrt{\int_{\Omega} F(\phi) d\mathbf{x} + C_0}, \quad (2.1)$$

where $F(\phi) = \frac{1}{4}\phi^4 - \frac{S+\varepsilon}{2}\phi^2$ with $S \geq 0$, and C_0 is a positive constant such that $E_1(\phi) + C_0 > 0$. In this paper, we further assume that C_0 is large enough such that

$$\frac{C_0}{2} \leq E_1(\phi) + C_0 \leq 2C_0. \quad (2.2)$$

Then, an equivalent system of the original problem (1.2) with scalar auxiliary variable is given as

$$\begin{cases} \frac{\partial \phi}{\partial t} = \Delta \mu, \\ \mu = (\Delta + \beta)^2 \phi + S\phi + \frac{r(t)}{\sqrt{E_1(\phi) + C_0}} F'(\phi), \\ \frac{dr}{dt} = \frac{1}{2\sqrt{E_1(\phi) + C_0}} \int_{\Omega} F'(\phi) \frac{\partial \phi}{\partial t} d\mathbf{x}. \end{cases} \quad (2.3)$$

(2.3) satisfies the following energy dissipation law

$$\frac{d\overline{E}(\phi, r)}{dt} = -\|\nabla \mu\|^2 \leq 0, \quad (2.4)$$

where $\overline{E}(\phi, r) := \frac{1}{2}\|(\Delta + \beta)\phi\|^2 + \frac{S}{2}\|\phi\|^2 + r^2$. Moreover, we have

$$\overline{E}(\phi, r) \leq \overline{E}(\phi_0(\mathbf{x}), r(0)), \quad (2.5)$$

which shows the H^2 bound of the solution of (2.3). From the definition of the auxiliary variable $r(t)$ in (2.1), it follows that $\overline{E}(\phi, r) = E(\phi) + C_0$, which indicates that the energy dissipation law (2.4) is the same as (1.3).

We are now ready to construct efficient time stepping schemes for (2.3) to numerically approximate the solution ϕ on the nonuniform temporal mesh. Let $\tau_n := t_n - t_{n-1}$, $n = 1, 2, \dots, M$ be the time step size, $\gamma_{n+1} = \tau_{n+1}/\tau_n$ be the adjacent time-step ratio, and $\tau = \max\{\tau_n, n = 1, 2, \dots, M\}$ be the maximum time step size of the temporal mesh.

2.1. A second-order BDF scheme on nonuniform temporal mesh. We firstly recall the first order scheme for solving (2.3) reported in [20]

$$\frac{\phi^{n+1} - \phi^n}{\tau_{n+1}} = \Delta \mu^{n+1}, \quad (2.6a)$$

$$\mu^{n+1} = (\Delta + \beta)^2 \phi^{n+1} + S \phi^{n+1} + \frac{r^{n+1}}{\sqrt{E_1^n + C_0}} F'(\phi^n), \quad (2.6b)$$

$$\frac{r^{n+1} - r^n}{\tau_{n+1}} = \frac{1}{2\sqrt{E_1^n + C_0}} \int_{\Omega} F'(\phi^n) \frac{\phi^{n+1} - \phi^n}{\tau_{n+1}} d\mathbf{x}, \quad (2.6c)$$

where ϕ^n is an approximation to $\phi(t_n)$ and $E_1^n := E_1(\phi^n)$. As stated in [20], the scheme (2.6) is unconditionally energy stable in the sense that the following discrete energy law holds

$$\overline{E}(\phi^{n+1}, r^{n+1}) - \overline{E}(\phi^n, r^n) \leq 0. \quad (2.7)$$

To construct a second-order BDF scheme for (2.3), we firstly introduce a second order approximation $F_2^{j+\sigma} \phi$ to $\phi(t)$ at $t = t_{j+\sigma}$ as follows, seeing also [13, 15]. Here, $t_{j+\sigma} := t_n + \sigma \tau_{n+1}$ with $\frac{1}{2} \leq \sigma \leq 1$.

$$F_2^{j+\sigma} \phi := \frac{1}{\tau_{j+1}} \left[\frac{1 + 2\sigma\gamma_{j+1}}{1 + \gamma_{j+1}} \phi^{j+1} - (1 + (2\sigma - 1)\gamma_{j+1}) \phi^j + \frac{(2\sigma - 1)\gamma_{j+1}^2}{1 + \gamma_{j+1}} \phi^{j-1} \right], \quad (2.8)$$

where ϕ^j is an approximation to $\phi(t_j)$. Note that when $\sigma = 1$, it becomes the classical second order BDF with variable time steps:

$$F_2^{j+1} \phi = \frac{1}{\tau_{j+1}} \left[\frac{1 + 2\gamma_{j+1}}{1 + \gamma_{j+1}} \phi^{j+1} - (1 + \gamma_{j+1}) \phi^j + \frac{\gamma_{j+1}^2}{1 + \gamma_{j+1}} \phi^{j-1} \right], \quad (2.9)$$

and Crank-Nicolson formula

$$F_2^{j+1/2} \phi = \frac{\phi^{j+1} - \phi^j}{\tau_{j+1}}$$

for $\sigma = \frac{1}{2}$.

Now, we are ready to construct the second-order BDF scheme on nonuniform temporal mesh for the PFC system (2.3),

$$F_2^{n+\sigma} \phi = \Delta \mu^{n+\sigma}, \quad (2.10a)$$

$$\mu^{n+\sigma} = (\Delta + \beta)^2 \phi^{n+\sigma} + S \phi^{n+\sigma} + \frac{r^{n+1}}{\sqrt{E_1^n + C_0}} F'(\phi^{*,n+\sigma}), \quad (2.10b)$$

$$\frac{r^{n+1} - r^n}{\tau_{n+1}} = \frac{1}{2\sqrt{E_1^n + C_0}} \int_{\Omega} F'(\phi^{*,n+\sigma}) \frac{\phi^{n+1} - \phi^n}{\tau_{n+1}} d\mathbf{x}, \quad (2.10c)$$

where $\phi^{n+\sigma} := \sigma \phi^{n+1} + (1 - \sigma) \phi^n$ and $\phi^{*,n+\sigma} := \phi^n + \sigma \gamma_{n+1} (\phi^n - \phi^{n-1})$. Though only the first order finite difference approximation is used in (2.10c), we will see in section 3, the proposed scheme (2.10) is actually of second order accuracy for ϕ with $C_0 \geq 1/\tau$.

Before rigorously proving the energy stability of the scheme (2.10), we need the following essential inequality, seeing also [13, 15],

$$\delta_t \phi^{n+1} \cdot F_2^{n+\sigma} \phi \geq \left[g(\gamma_{n+2}) + \frac{1}{2} G(\gamma_{n+1}, \gamma_{n+2}) \right] \frac{|\delta_t \phi^{n+1}|^2}{\tau_{n+1}} - g(\gamma_{n+1}) \frac{|\delta_t \phi^n|^2}{\tau_n}, \quad (2.11)$$

where $\delta_t \phi^{n+1} = \phi^{n+1} - \phi^n$. And in (2.11), for any $0 < s, z \leq \gamma_{**}(\sigma)$,

$$g(\gamma_{n+1}) := \frac{(2\sigma - 1)\gamma_{n+1}^{\frac{3}{2}}}{2(1 + \gamma_{n+1})} > 0$$

and

$$G(s, z) := \frac{2 + 4\sigma s - (2\sigma - 1)s^{\frac{3}{2}}}{1 + s} - \frac{(2\sigma - 1)z^{\frac{3}{2}}}{1 + z} \geq 0.$$

Here $\gamma_{**}(\sigma)$ is the positive root of $G(z, z) = 0$. Moreover, the root function $\gamma_{**}(\sigma)$ is decreasing for $\sigma \in [\frac{1}{2}, 1]$ with $\gamma_{**}(1) \approx 4.8645$ and $\gamma_{**}(\sigma) \rightarrow +\infty$, as $\sigma \rightarrow \frac{1}{2}$. Thus $\gamma_{**}(\sigma) \geq 4.8645$ for any $\sigma \in [\frac{1}{2}, 1]$. Furthermore, for $4 \leq \gamma_*(\sigma) < \gamma_{**}(\sigma)$, it holds

$$G(s, z) \geq \min\{G(0, \gamma_*(\sigma)), G(\gamma_*(\sigma), \gamma_*(\sigma))\} \geq G(\gamma_*(\sigma), \gamma_*(\sigma)) > 0$$

for any $0 < s, z \leq \gamma_*(\sigma) < \gamma_{**}(\sigma)$.

To prove the following theorem on the unconditional energy stability of the scheme (2.10), we further introduce the inverse Laplace operator $\psi = (-\Delta)^{-1}u$ for $u \in L^2(\Omega)$ and $\int_{\Omega} u d\mathbf{x} = 0$, as defined in [28]:

$$\begin{cases} -\Delta \psi = u, \\ \int_{\Omega} \psi d\mathbf{x} = 0. \end{cases}$$

Theorem 2.1. *For $1/2 \leq \sigma \leq 1$ and $0 < \gamma_{n+1} \leq \gamma_{**}(\sigma)$, $n = 1, \dots, M-1$, it holds for the scheme (2.10) that*

$$\tilde{E}^{n+1} - \tilde{E}^n \leq 0, \quad (2.12)$$

where the discrete modified energy \tilde{E}^n is defined by:

$$\tilde{E}^n := \overline{E}(\phi^n, r^n) + \frac{(2\sigma - 1)\gamma_{n+1}^{\frac{3}{2}}}{2 + 2\gamma_{n+1}} \frac{\|\nabla^{-1}(\phi^n - \phi^{n-1})\|^2}{\tau_n}.$$

Proof. Taking the inner products of (2.10a) and (2.10b) with $(-\Delta)^{-1}\delta_t \phi^{n+1}$, $\delta_t \phi^{n+1}$ respectively, and multiplying (2.10c) with $2r^{n+1}$, we obtain

$$\begin{aligned} & \left(\nabla^{-1} F_2^{n+\sigma} \phi, \nabla^{-1} \delta_t \phi^{n+1} \right) = -(\mu^{n+\sigma}, \delta_t \phi^{n+1}), \\ & \left(\mu^{n+\sigma}, \delta_t \phi^{n+1} \right) = ((\Delta + \beta)\phi^{n+\sigma}, (\Delta + \beta)\delta_t \phi^{n+1}) + S(\phi^{n+\sigma}, \delta_t \phi^{n+1}) \\ & \quad + \frac{r^{n+1}}{\sqrt{E_1^n + C_0}} \left(F'(\phi^{*,n+1}), \delta_t \phi^{n+1} \right), \\ & \frac{2r^{n+1}(r^{n+1} - r^n)}{\tau_{n+1}} = \frac{r^{n+1}}{\sqrt{E_1^n + C_0}} \int_{\Omega} F'(\phi^{*,n+1}) \frac{\delta_t \phi^{n+1}}{\tau_{n+1}} d\mathbf{x}. \end{aligned}$$

From the above equations, it follows that

$$\begin{aligned} & \left(\nabla^{-1} F_2^{n+\sigma} \phi, \nabla^{-1} \delta_t \phi^{n+1} \right) + ((\Delta + \beta)\phi^{n+\sigma}, (\Delta + \beta)\delta_t \phi^{n+1}) \\ & + S(\phi^{n+\sigma}, \delta_t \phi^{n+1}) + 2r^{n+1}(r^{n+1} - r^n) = 0. \end{aligned} \quad (2.13)$$

Combining the inequality (2.11) and

$$\begin{aligned} 2a^{k+\sigma}(a^{k+1} - a^k) &= |a^{k+1}|^2 - |a^k|^2 + (2\sigma - 1)|a^k - a^{k-1}|^2, \\ 2a^{k+1}(a^{k+1} - a^k) &= |a^{k+1}|^2 - |a^k|^2 + |a^{k+1} - a^k|^2, \end{aligned} \quad (2.14)$$

we can easily derive the modified discrete energy law (2.12) from (2.13). Then we complete the proof. \square

2.2. Fully discrete scheme with Fourier spectral method. In this work, we only present the results in the two dimensional space. The results in the three dimensional space can be obtained in a similar way.

Let $\Omega := (0, L)^2$ and we use the uniform Fourier mode number of $2N + 1$ for each direction. The trial and test function space of the Fourier spectral method is defined by

$$X_N := \text{span}\{e^{i2(kx+ly)\pi/L} : -N \leq k, l \leq N\},$$

where $i = \sqrt{-1}$. By taking the Fourier spectral discretization in space, we can have the following fully discrete scheme of the semi-discrete approach (2.10): finding $\phi_N^{n+1} \in X_N$ and r^{n+1} such that

$$(F_2^{n+\sigma} \phi_N, p_N) = -(\nabla \mu_N^{n+\sigma}, \nabla p_N), \quad \forall p_N \in X_N, \quad (2.15a)$$

$$\begin{aligned} (\mu_N^{n+\sigma}, q_N) &= ((\Delta + \beta) \phi_N^{n+\sigma}, (\Delta + \beta) q_N) + S(\phi_N^{n+\sigma}, q_N) \\ &\quad + \frac{r^{n+1}}{\sqrt{E_{1,N}^n + C_0}} (F'(\phi_N^{*,n+\sigma}), q_N), \quad \forall q_N \in X_N \end{aligned} \quad (2.15b)$$

$$\frac{r^{n+1} - r^n}{\tau_{n+1}} = \frac{1}{2\sqrt{E_{1,N}^n + C_0}} \int_{\Omega} F'(\phi_N^{*,n+\sigma}) \frac{\phi_N^{n+1} - \phi_N^n}{\tau_{n+1}} d\mathbf{x}, \quad (2.15c)$$

where $E_{1,N}^n := E_1(\phi_N^n)$, $\phi_N^{n+\sigma} := \sigma \phi_N^{n+1} + (1 - \sigma) \phi_N^n$ and $\phi_N^{*,n+\sigma} := \phi_N^n + \sigma \gamma_{n+1} (\phi_N^n - \phi_N^{n-1})$.

Since the proof of the unconditional energy stability for (2.15) is essentially similar to that of the semi-discrete scheme (2.10), we only state the following theorem and omit the proof.

Theorem 2.2. *For the fully discrete scheme (2.15), if $1/2 \leq \sigma \leq 1$ and $0 < \gamma_{n+1} \leq \gamma_{**}(\sigma)$, $n = 1, 2, \dots, M - 1$, we have*

$$\tilde{E}_N^{n+1} - \tilde{E}_N^n \leq 0, \quad (2.16)$$

where \tilde{E}_N^n is defined by:

$$\tilde{E}_N^n := \overline{E}(\phi_N^n, r^n) + \frac{(2\sigma - 1)\gamma_{n+1}^{\frac{3}{2}} \|\nabla^{-1}(\phi_N^n - \phi_N^{n-1})\|^2}{2 + 2\gamma_{n+1} \tau_n}.$$

3. ERROR ANALYSIS

In this section, we establish a rigorous error estimate for the fully discrete scheme (2.15) with a mild smoothness requirement on the exact solution. For simplicity, we only focus our attention on the investigation of the numerical solutions for the special case with $\sigma = 1$ in what follows, and

the obtained results are also right for the general parameter $\sigma \in [1/2, 1]$. We denote $\gamma_* := \gamma_*(1)$. From (2.16), we can deduce that for any $\phi_0(\mathbf{x}) \in H^2(\Omega)$ and $0 < \gamma_n \leq \gamma_*$,

$$\|(\Delta + \beta)\phi_N^n\| + \|\phi_N^n\| + |r^n| \leq \mathcal{M}, \quad n = 1, 2, \dots, M \quad (3.1)$$

for the fully discrete second order scheme (2.15). Here \mathcal{M} is a positive constant only depending on Ω and the initial condition $\phi_0(\mathbf{x})$. This indicates the H^2 bound of the numerical solution and the uniform bound of the auxiliary variable r^n for all $n = 1, 2, \dots, M$.

We recall the L^2 orthogonal projection $\Pi_N: L^2(\Omega) \rightarrow X_N$, defined by

$$(\Pi_N u - u, v) = 0, \quad \forall v \in X_N. \quad (3.2)$$

It is obvious that $\Pi_N u$ is the truncated Fourier series, namely

$$\Pi_N u = \sum_{k,l=-N}^N \hat{u}_{k,l} e^{i2(kx+ly)\pi/L},$$

with

$$\hat{u}_{k,l} = (u, e^{i2(kx+ly)\pi/L}) = \frac{1}{|\Omega|} \int_{\Omega} u(x, y) e^{-i2(kx+ly)\pi/L} dx dy.$$

For this L^2 orthogonal projection Π_N , we have the following optimal estimate, seeing also [24],

$$\|\Pi_N u - u\|_{\mu} \leq C N^{\mu-m} \|u\|_m, \quad (3.3)$$

for any $u \in H_{per}^m(\Omega)$ and $0 \leq \mu \leq m$. Here $H_{per}^m(\Omega)$ is the subspace of $H^m(\Omega)$, which consists of functions with derivatives of order up to $m-1$ being L -periodic. We denote $\bar{e}_u^n := u_N^n - \Pi_N u(t_n)$ with $\bar{e}_u^0 = 0$, $\hat{e}_u^n := \Pi_N u(t_n) - u(t_n)$, $e_r^n := r^n - r(t_n)$ and $\phi(t_{*,n+1}) := \phi(t_n) + \gamma_{n+1}(\phi(t_n) - \phi(t_{n-1}))$. Then we have

$$e_{\phi}^n := \phi_N^n - \phi(t_n) = \bar{e}_{\phi}^n + \hat{e}_{\phi}^n, \quad e_{\mu}^n := \mu_N^n - \mu(t_n) = \bar{e}_{\mu}^n + \hat{e}_{\mu}^n.$$

For simplicity, we also denote $\delta_t \bar{e}_u^n := \bar{e}_u^n - \bar{e}_u^{n-1}$. The error estimates of ϕ_N^n and r^n are derived in the following theorem.

Theorem 3.1. *Assume that $\phi^0 := \phi(\mathbf{x}, 0) \in H^2(\Omega)$, $0 < \gamma_n \leq \gamma_*$, $\tau_1 \leq C\tau^{\frac{4}{3}}$, and $F(\cdot) \in C^3(\mathbb{R})$. Provided that*

$$\begin{aligned} \phi &\in L^{\infty}(0, T; H_{per}^m), \phi_t \in L^{\infty}(0, T; H_{per}^m) \cap L^2(0, T; H^1), \\ \phi_{tt} &\in L^2(0, T; H^1), \phi_{ttt} \in L^2(0, T; H^{-1}) \end{aligned} \quad (3.4)$$

for $m \geq 2$, it holds

$$\begin{aligned} &\frac{\gamma_{n+2}^{\frac{3}{2}}}{2(1 + \gamma_{n+2})} \frac{\|\nabla^{-1}(e_{\phi}^{n+1} - e_{\phi}^n)\|^2}{\tau_{n+1}} + \frac{1}{2} \|(\Delta + \beta)e_{\phi}^{n+1}\|^2 + \frac{S}{2} \|e_{\phi}^{n+1}\|^2 + |e_r^{n+1}|^2 \\ &\leq C \exp(T) \left[\frac{\tau^2}{C_0} \int_0^T (\|\phi_t(s)\|_{H^1}^2 + \|\phi_{tt}(s)\|^2) ds + \tau^4 \int_0^T (\|\phi_{tt}(s)\|_{H^1}^2 \right. \\ &\quad \left. + \|\phi_{ttt}(s)\|_{H^{-1}}^2) ds + T \left(N^{-2m} \|\phi_t\|_{L^{\infty}(0, T; H^m)}^2 + N^{4-2m} \|\phi\|_{L^{\infty}(0, T; H^m)} \right) \right]. \end{aligned} \quad (3.5)$$

Moreover, we have

$$\begin{aligned}
 & \frac{\gamma_{n+2}^{\frac{3}{2}}}{2(1+\gamma_{n+2})} \frac{\|\nabla^{-1}(e_\phi^{n+1} - e_\phi^n)\|^2}{\tau_{n+1}} + \frac{1}{2}\|(\Delta + \beta)e_\phi^{n+1}\|^2 + \frac{S}{2}\|e_\phi^{n+1}\|^2 \\
 & \leq C \exp(T) \left[\frac{\tau^2}{C_0^2} \int_0^T (\|\phi_t(s)\|_{H^1}^2 + \|\phi_{tt}(s)\|^2) ds + \tau^4 \int_0^T (\|\phi_{tt}(s)\|_{H^1}^2 \right. \\
 & \quad \left. + \|\phi_{ttt}(s)\|_{H^{-1}}^2) ds + T \left(N^{-2m} \|\phi_t\|_{L^\infty(0,T;H^m)}^2 + N^{4-2m} \|\phi\|_{L^\infty(0,T;H^m)}^2 \right) \right],
 \end{aligned} \tag{3.6}$$

and if we set the positive constant C_0 large enough such that $C_0 \geq \frac{1}{\tau}$, it holds

$$\begin{aligned}
 & \frac{\gamma_{n+2}^{\frac{3}{2}}}{2(1+\gamma_{n+2})} \frac{\|\nabla^{-1}(e_\phi^{n+1} - e_\phi^n)\|^2}{\tau_{n+1}} + \frac{1}{2}\|(\Delta + \beta)e_\phi^{n+1}\|^2 + \frac{S}{2}\|e_\phi^{n+1}\|^2 \\
 & \leq C \exp(T) \left[\tau^4 \int_0^T (\|\phi_t(s)\|_{H^1}^2 + \|\phi_{tt}(s)\|_{H^1}^2 + \|\phi_{ttt}(s)\|_{H^{-1}}^2) ds \right. \\
 & \quad \left. + T \left(N^{-2m} \|\phi_t\|_{L^\infty(0,T;H^m)}^2 + N^{4-2m} \|\phi\|_{L^\infty(0,T;H^m)}^2 \right) \right].
 \end{aligned} \tag{3.7}$$

Proof. From (2.5), (3.1) and the Sobolev embedding theorem, $H^2 \subset L^\infty$, it follows that $\|\phi(t)\|_{L^\infty}$, $\|\phi^n\|_{L^\infty} \leq C$, where the positive constant C only depends on ϕ^0, Ω and T . Combining the definition of $F(\cdot)$, we have

$$\|F(\cdot)\|_{L^\infty}, \|F'(\cdot)\|_{L^\infty}, \|F''(\cdot)\|_{L^\infty}, \|F'''(\cdot)\|_{L^\infty} \leq C, \tag{3.8}$$

for ϕ and $\phi^n, n = 0, 1, 2, \dots, M$. In what follows, we use $\mathcal{A} \lesssim \mathcal{B}$ to represent that $\mathcal{A} \leq C\mathcal{B}$, where the general positive constant C is independent of C_0 . From the definition of $r(t)$ in (2.1), we can derive

$$r_{tt} = -\frac{(\int_\Omega F'(\phi)\phi_t d\mathbf{x})^2}{4\sqrt{(E_1(\phi) + C_0)^3}} + \frac{\int_\Omega [F''(\phi)\phi_t^2 + F'(\phi)\phi_{tt}] d\mathbf{x}}{2\sqrt{E_1(\phi) + C_0}}.$$

Moreover, together with (2.2), (3.4) and (3.8), and using Hölder inequality, we can deduce that

$$\int_{t_n}^{t_{n+1}} |r_{tt}|^2 dt \lesssim \frac{1}{C_0} \int_{t_n}^{t_{n+1}} (\|\phi_t\|_{L^4}^2 + \|\phi_{tt}\|^2) dt \lesssim \frac{1}{C_0} \int_{t_n}^{t_{n+1}} (\|\phi_t\|_{H^1}^2 + \|\phi_{tt}\|^2) dt, \tag{3.9}$$

where we have used the Sobolev embedding theorem, $H^1 \subset L^4$. From (2.3), (2.10) and the definition of the L^2 orthogonal projection $\Pi_n \phi(t_n)$ in (3.2), we derive the following error equation for $n \geq 1$:

$$(F_2^{n+1} \bar{e}_\phi, p_N) + (\nabla \bar{e}_\mu^{n+1}, \nabla p_N) = (T_1^n, p_N), \tag{3.10a}$$

$$\begin{aligned}
 (\bar{e}_\mu^{n+1}, q_N) &= ((\Delta + \beta) \bar{e}_\phi^{n+1}, (\Delta + \beta) q_N) + S(\bar{e}_\phi^{n+1}, q_N) \\
 &+ \frac{e_r^{n+1}}{\sqrt{E_{1,N}^n + C_0}} (F'(\phi_N^{*,n+1}), q_N) + (J_1^n + T_2^n, q_N),
 \end{aligned} \tag{3.10b}$$

$$\begin{aligned}
 e_r^{n+1} - e_r^n &= \frac{1}{2\sqrt{E_1^n + C_0}} \int_\Omega F'(\phi_N^{*,n+1}) (\bar{e}_\phi^{n+1} - \bar{e}_\phi^n) d\mathbf{x} \\
 &+ \int_\Omega J_2^n \cdot (\Pi_N(\phi(t_{n+1}) - \phi(t_n))) d\mathbf{x} + J_3^n - v_1^n + v_2^n,
 \end{aligned} \tag{3.10c}$$

where

$$\begin{aligned} J_1^n &:= r(t_{n+1}) \left[\frac{F'(\phi_N^{*,n+1})}{\sqrt{E_{1,N}^n + C_0}} - \frac{F'(\phi(t_{*,n+1}))}{\sqrt{E_1(\phi(t_{n+1})) + C_0}} \right], \\ J_2^n &:= \frac{1}{2} \left[\frac{F'(\phi_N^{*,n+1})}{\sqrt{E_{1,N}^n + C_0}} - \frac{F'(\phi(t_{n+1}))}{\sqrt{E_1(\phi(t_{n+1})) + C_0}} \right], \\ J_3^n &:= \int_{\Omega} \frac{F'(\phi(t_{n+1}))}{2\sqrt{E_1(\phi(t_{n+1})) + C_0}} (\widehat{e}_{\phi}^{n+1} - \widehat{e}_{\phi}^n) d\mathbf{x}, \end{aligned}$$

and the truncation errors are defined by

$$T_1^n = \phi(t_{n+1}) - \partial_t(\Pi_{2,n}\phi(t))|_{t=t_{n+1}}, \quad T_2^n = F'(\phi(t_{*,n+1})) - F'(\phi(t_{n+1})) \quad (3.11a)$$

$$v_1^n = r(t_{n+1}) - r(t_n) - \tau_{n+1}r_t(t_{n+1}) = \int_{t_n}^{t_{n+1}} (t_n - s)r_{tt}(s)ds, \quad (3.11b)$$

$$v_2^n = \left(\frac{F'(\phi(t_{n+1}))}{2\sqrt{E_1(\phi(t_{n+1})) + C_0}}, \int_{t_n}^{t_{n+1}} (t_n - s)\phi_{tt}(s)ds \right). \quad (3.11c)$$

Here, $\Pi_{2,n}\phi(t)$ denotes the quadratic interpolation polynomial associated with $(t_{n-1}, \phi(t_{n-1}))$, $(t_n, \phi(t_n))$ and $(t_{n+1}, \phi(t_{n+1}))$. Taking $p_N = (-\Delta)^{-1}(\delta_t \bar{e}_{\phi}^{n+1})$ and $q_N = \delta_t \bar{e}_{\phi}^{n+1}$ into (3.10a) and (3.10b), respectively, and multiplying (3.10c) with $2e_r^{n+1}$, we sum them up to derive

$$\begin{aligned} & (\nabla^{-1}F_2^{n+1}\bar{e}_{\phi}, \nabla^{-1}\delta_t \bar{e}_{\phi}^{n+1}) + ((\Delta + \beta)\bar{e}_{\phi}^{n+1}, (\Delta + \beta)\delta_t \bar{e}_{\phi}^{n+1}) + S(\bar{e}_{\phi}^{n+1}, \delta_t \bar{e}_{\phi}^{n+1}) \\ & + 2e_r^{n+1}(e_r^{n+1} - e_r^n) \\ = & -(J_1^n + T_2^n, \delta_t \bar{e}_{\phi}^{n+1}) + (\nabla^{-1}T_1^n, \nabla^{-1}\delta_t \bar{e}_{\phi}^{n+1}) \\ & + 2e_r^{n+1} \int_{\Omega} J_2^n \cdot \Pi_N(\phi(t_{n+1}) - \phi(t_n)) d\mathbf{x} + 2e_r^{n+1}J_3^n + 2e_r^{n+1}(-v_1^n + v_2^n). \end{aligned}$$

Using (2.11), the identities (2.14), and Young's inequality, we derive

$$\begin{aligned} & \frac{1}{2} \left[\left(\frac{\gamma_{n+2}^{\frac{3}{2}}}{1 + \gamma_{n+2}} + G(\gamma_*, \gamma_*) \right) \frac{\|\nabla^{-1}\delta_t \bar{e}_{\phi}^{n+1}\|^2}{\tau_{n+1}} - \frac{\gamma_{n+1}^{\frac{3}{2}}}{1 + \gamma_{n+1}} \frac{\|\nabla^{-1}\delta_t \bar{e}_{\phi}^n\|^2}{\tau_n} \right] \\ & + \frac{1}{2} [\|(\Delta + \beta)\bar{e}_{\phi}^{n+1}\|^2 - \|(\Delta + \beta)\bar{e}_{\phi}^n\|^2] + \frac{S}{2} [\|\bar{e}_{\phi}^{n+1}\|^2 - \|\bar{e}_{\phi}^n\|^2] + |e_r^{n+1}|^2 - |e_r^n|^2 \\ \leq & C(\gamma_*)\tau_{n+1} [\|\nabla J_1^n\|^2 + \|\nabla^{-1}T_1^n\|^2 + \|\nabla T_2^n\|^2] + G(\gamma_*, \gamma_*) \frac{\|\nabla^{-1}\delta_t \bar{e}_{\phi}^{n+1}\|^2}{2\tau_{n+1}} \\ & + C\tau_{n+1} \|\phi_t\|_{L^\infty(0,T;L^2)} [|e_r^{n+1}|^2 + \|J_2^n\|^2] + \frac{C\tau_{n+1}}{\sqrt{C_0}} [|e_r^{n+1}|^2 \\ & + N^{-2m} \|\phi_t\|_{L^\infty(0,T;H^m)}^2] + \tau_{n+1}|e_r^{n+1}|^2 + \frac{2}{\tau_{n+1}} (|v_1^n|^2 + |v_2^n|^2), \end{aligned}$$

where we have used

$$\begin{aligned}
 & 2e_r^{n+1} \cdot J_3^n \\
 & \leq \frac{\|F'(\phi(t_{n+1}))\|_{L^\infty}}{\sqrt{E_1(\phi(t_{n+1}))} + C_0} \int_{\Omega} e_r^{n+1} (\widehat{e}_\phi^{n+1} - \widehat{e}_\phi^n) d\mathbf{x} \\
 & \leq \frac{C}{\sqrt{C_0}} \left[\tau_{n+1} |e_r^{n+1}|^2 + \frac{1}{\tau_{n+1}} \int_{\Omega} |\widehat{e}_\phi^{n+1} - \widehat{e}_\phi^n|^2 d\mathbf{x} \right] \\
 & = \frac{C}{\sqrt{C_0}} \left[\tau_{n+1} |e_r^{n+1}|^2 + \frac{1}{\tau_{n+1}} \int_{\Omega} |\Pi_N(\phi(t_{n+1}) - \phi(t_n)) - (\phi(t_{n+1}) - \phi(t_n))|^2 d\mathbf{x} \right] \\
 & \leq \frac{C}{\sqrt{C_0}} \left[\tau_{n+1} |e_r^{n+1}|^2 + \tau_{n+1} N^{-2m} \|\phi_t\|_{L^\infty(0,T;H^m)}^2 \right].
 \end{aligned}$$

Combining with (3.4), we have following error inequality

$$\begin{aligned}
 & \frac{1}{2} \left[\frac{\gamma_{n+2}^{\frac{3}{2}}}{1 + \gamma_{n+2}} \frac{\|\nabla^{-1} \delta_t \bar{e}_\phi^{n+1}\|^2}{\tau_{n+1}} - \frac{\gamma_{n+1}^{\frac{3}{2}}}{1 + \gamma_{n+1}} \frac{\|\nabla^{-1} \delta_t \bar{e}_\phi^n\|^2}{\tau_n} \right] + \frac{1}{2} [\|(\Delta + \beta) \bar{e}_\phi^{n+1}\|^2 \\
 & - \|(\Delta + \beta) \bar{e}_\phi^n\|^2] + \frac{S}{2} [\|\bar{e}_\phi^{n+1}\|^2 - \|\bar{e}_\phi^n\|^2] + |e_r^{n+1}|^2 - |e_r^n|^2 \\
 & \lesssim \tau_{n+1} \left[\|\nabla J_1^n\|^2 + \|J_2^n\|^2 + |e_r^{n+1}|^2 + \|\nabla^{-1} T_1^n\|^2 + \|\nabla T_2^n\|^2 \right. \\
 & \left. + N^{-2m} \|\phi_t\|_{L^\infty(0,T;H^m)}^2 \right] + \frac{2(|v_1^n|^2 + |v_2^n|^2)}{\tau_{n+1}}.
 \end{aligned} \tag{3.12}$$

Moreover, we have

$$\nabla J_1^n = -r(t_{n+1}) \left[\frac{\nabla I_1^n}{\sqrt{E_{1,N}^n} + C_0} + \nabla F'(\phi(t_{*,n+1})) \cdot I_2^n \right], \tag{3.13}$$

where

$$I_1^n := F'(\phi_N^{*,n+1}) - F'(\phi(t_{*,n+1})), \quad I_2^n := \frac{1}{\sqrt{E_{1,N}^n} + C_0} - \frac{1}{\sqrt{E_1(\phi(t_{n+1}))} + C_0}. \tag{3.14}$$

From (3.8) and $\phi(t_{*,n+1}) \in H^2$, it follows that

$$\begin{aligned}
 \|\nabla F'(\phi(t_{*,n+1}))\| &= \|F''(\phi(t_{*,n+1})) \nabla \phi(t_{*,n+1})\| \\
 &\leq \|F''(\phi(t_{*,n+1}))\|_{L^\infty} \|\nabla \phi(t_{*,n+1})\| \leq C.
 \end{aligned}$$

Therefore, together with (2.1) and (2.2), we deduce that

$$\|\nabla J_1^n\|^2 \lesssim [\|\nabla I_1^n\|^2 + C_0 |I_2^n|^2]. \tag{3.15}$$

For the term J_2^n , using triangle inequality and (2.2), we have

$$\begin{aligned}
 \|J_2^n\|^2 &= \frac{1}{2} \left\| \frac{I_1^n}{\sqrt{E_{1,N}^n} + C_0} + \frac{T_2^n}{\sqrt{E_{1,N}^n} + C_0} + F'(\phi(t_{n+1})) \cdot I_2^n \right\|^2 \\
 &\lesssim \frac{\|I_1^n\|^2}{C_0} + \frac{\|T_2^n\|^2}{C_0} + |I_2^n|^2.
 \end{aligned} \tag{3.16}$$

Then, we substitute the estimates (3.15) and (3.16) into the error inequality (3.12) to get

$$\begin{aligned}
& \frac{\gamma_{n+2}^{\frac{3}{2}}}{1 + \gamma_{n+2}} \frac{\|\nabla^{-1} \delta_t \bar{e}_\phi^{n+1}\|^2}{2\tau_{n+1}} - \frac{\gamma_{n+1}^{\frac{3}{2}}}{1 + \gamma_{n+1}} \frac{\|\nabla^{-1} \delta_t \bar{e}_\phi^n\|^2}{2\tau_n} + \frac{1}{2} [\|(\Delta + \beta) \bar{e}_\phi^{n+1}\|^2 \\
& - \|(\Delta + \beta) \bar{e}_\phi^n\|^2] + \frac{S}{2} [\|\bar{e}_\phi^{n+1}\|^2 - \|\bar{e}_\phi^n\|^2] + |e_r^{n+1}|^2 - |e_r^n|^2 \\
& \lesssim \tau_{n+1} \left[|e_r^{n+1}|^2 + \frac{1}{C_0} \|I_1^n\|^2 + \|\nabla I_1^n\|^2 + C_0 |I_2^n|^2 + \|\nabla^{-1} T_1^n\|^2 + \frac{1}{C_0} \|T_2^n\|^2 \right. \\
& \left. + \|\nabla T_2^n\|^2 + N^{-2m} \|\phi_t\|_{L^\infty(0,T;H^m)}^2 \right] + \frac{2}{\tau_{n+1}} (|v_1^n|^2 + |v_2^n|^2).
\end{aligned} \tag{3.17}$$

Moreover, from (3.14), (3.8), (3.3) and (2.2),

$$\begin{aligned}
\|I_1^n\|^2 &= \|F'(\phi_N^{*,n+1}) - F'(\phi(t_{*,n+1}))\|^2 \lesssim \|e_\phi^n\|^2 + \|e_\phi^{n-1}\|^2, \\
&\lesssim \|\bar{e}_\phi^n + \hat{e}_\phi^n\|^2 + \|\bar{e}_\phi^{n-1} + \hat{e}_\phi^{n-1}\|^2 \\
&\lesssim \|\bar{e}_\phi^n\|^2 + \|\bar{e}_\phi^{n-1}\|^2 + N^{-2m} \|\phi\|_{L^\infty(0,T;H^m)}, \\
|I_2^n|^2 &= \left| \frac{E_1(\phi(t_{n+1})) - E_{1,N}^n}{\mathcal{G}(C_0)} \right|^2 \lesssim \frac{1}{C_0^3} |E_1(\phi(t_{n+1})) - E_{1,N}^n|^2 \\
&\lesssim \frac{1}{C_0^3} \left(|E_1(\phi(t_{n+1})) - E_1(\phi(t_n))|^2 + |E_1(\phi(t_n)) - E_{1,N}^n|^2 \right) \\
&\lesssim \frac{1}{C_0^3} \left(\tau_{n+1} \int_{t_n}^{t_{n+1}} \|\phi_t(s)\|^2 ds + \|e_\phi^n\|^2 \right) \\
&\lesssim \frac{1}{C_0^3} \left(\tau_{n+1} \int_{t_n}^{t_{n+1}} \|\phi_t(s)\|^2 ds + \|\bar{e}_\phi^n\|^2 + N^{-2m} \|\phi\|_{L^\infty(0,T;H^m)}^2 \right),
\end{aligned} \tag{3.18}$$

where the $\mathcal{G}(C_0)$ is defined by

$$\mathcal{G}(C_0) := \sqrt{E_{1,N}^n + C_0} \sqrt{E_1(\phi(t_{n+1})) + C_0} \left(\sqrt{E_1(\phi(t_{n+1})) + C_0} + \sqrt{E_{1,N}^n + C_0} \right).$$

From the definition of I_1^n in (3.14), we have

$$\|\nabla I_1^n\|^2 = \|I_{1,1}^n + I_{1,2}^n\|^2 \leq \|I_{1,1}^n\|^2 + \|I_{1,2}^n\|^2, \tag{3.19}$$

where $I_{1,1}^n$ and $I_{1,2}^n$ are defined by

$$\begin{aligned}
I_{1,1}^n &:= F''(\phi_N^{*,n+1}) \nabla (\phi_N^{*,n+1} - \phi(t_{*,n+1})), \\
I_{1,2}^n &:= (F''(\phi_N^{*,n+1}) - F''(\phi(t_{*,n+1}))) \nabla \phi(t_{*,n+1}).
\end{aligned}$$

Furthermore, using (3.8), the Hölder's inequality and the Sobolev embedding theorem, $H^1 \subset L^6$, we have

$$\begin{aligned}
\|I_{1,1}^n\|^2 &\lesssim \|\nabla e_\phi^n\|^2 + \|\nabla e_\phi^{n-1}\|^2 \\
\|I_{1,2}^n\|^2 &\lesssim \|(\phi_N^{*,n+1} - \phi(t_{*,n+1})) \nabla \phi(t_{*,n+1})\|^2 \\
&\lesssim \|\phi_N^{*,n+1} - \phi(t_{*,n+1})\|_{L^6}^2 \|\nabla \phi(t_{*,n+1})\|_{L^3}^2 \\
&\lesssim \|\phi_N^{*,n+1} - \phi(t_{*,n+1})\|_{H^1}^2 \|\phi(t_{*,n+1})\|_{H^2}^2 \\
&\lesssim \|e_\phi^n\|_{H^1}^2 + \|e_\phi^{n-1}\|_{H^1}^2.
\end{aligned} \tag{3.20}$$

Combining (3.19) and (3.20) gives

$$\begin{aligned}
 \|\nabla I_1^n\|^2 &\lesssim \|\nabla e_\phi^n\|^2 + \|\nabla e_\phi^{n-1}\|^2 + \|e_\phi^n\|^2 + \|e_\phi^{n-1}\|^2 \\
 &\lesssim \|\Delta \bar{e}_\phi^n\|^2 + \|\Delta \bar{e}_\phi^{n-1}\|^2 + \|\bar{e}_\phi^n\|^2 + \|\bar{e}_\phi^{n-1}\|^2 + N^{4-2m} \|\phi\|_{L^\infty(0,T;H^m)}^2, \\
 &\lesssim \|(\Delta + \beta) \bar{e}_\phi^n\|^2 + \|(\Delta + \beta) \bar{e}_\phi^{n-1}\|^2 + \|\bar{e}_\phi^n\|^2 + \|\bar{e}_\phi^{n-1}\|^2 + N^{4-2m} \|\phi\|_{L^\infty(0,T;H^m)}^2
 \end{aligned} \tag{3.21}$$

in which we have used

$$\begin{aligned}
 \|\nabla e_\phi^{n+1}\|^2 &= (-\Delta e_\phi^{n+1}, e_\phi^{n+1}) \leq \frac{\|\Delta e_\phi^{n+1}\|^2 + \|e_\phi^{n+1}\|^2}{2}, \\
 \|\Delta e_\phi^{n+1}\|^2 &= \|\Delta \bar{e}_\phi^{n+1} + \Delta \hat{e}_\phi^{n+1}\|^2 \leq \|\Delta \bar{e}_\phi^{n+1}\|^2 + CN^{4-2m} \|\phi\|_{L^\infty(0,T;H^m)}^2.
 \end{aligned}$$

For the truncation errors of T_1^n , T_2^n , v_1^n , and v_2^n , the following estimates hold, seeing also [2, 25],

$$\begin{aligned}
 \|\nabla^{-1} T_1^n\|^2 &\lesssim (\tau_n + \tau_{n+1})^3 \int_{t_{n-1}}^{t_{n+1}} \|\phi_{ttt}(s)\|_{H^{-1}}^2 ds, \\
 \|T_2^n\|^2 &\lesssim \|\phi(t_{n+1}) - \phi(t_{*,n+1})\|^2 \lesssim (\tau_n + \tau_{n+1})^3 \int_{t_{n-1}}^{t_{n+1}} \|\phi_{tt}(s)\|^2 ds, \\
 \|\nabla T_2^n\|^2 &\lesssim \|\phi(t_{n+1}) - \phi(t_{*,n+1})\|^2 + \|\nabla(\phi(t_{n+1}) - \phi(t_{*,n+1}))\|^2 \\
 &\lesssim (\tau_n + \tau_{n+1})^3 \int_{t_{n-1}}^{t_{n+1}} \|\phi_{tt}(s)\|_{H^1}^2 ds, \\
 |v_1^n|^2 &\leq \frac{1}{3} \tau_{n+1}^3 \int_{t_n}^{t_{n+1}} |r_{tt}(s)|^2 ds \lesssim \frac{\tau_{n+1}^3}{C_0} \int_{t_n}^{t_{n+1}} (\|\phi_t\|_{H^1}^2 + \|\phi_{tt}\|^2) dt, \\
 |v_2^n|^2 &\lesssim \tau_{n+1}^3 \left\| \frac{F'(\phi(t_{n+1}))}{2\sqrt{E_1(\phi(t_{n+1}))} + C_0} \right\|^2 \int_{t_n}^{t_{n+1}} \|\phi_{tt}(s)\|^2 ds \\
 &\lesssim \frac{\tau_{n+1}^3}{C_0} \int_{t_n}^{t_{n+1}} \|\phi_{tt}(s)\|^2 ds,
 \end{aligned} \tag{3.22}$$

where the estimate for r_{tt} in (3.9) is used. Then we take the above estimates (3.18)-(3.22) into (3.17), and sum up it from 1 to n to get

$$\begin{aligned}
 &\frac{\gamma_{n+2}^{\frac{3}{2}}}{2(1+\gamma_{n+2})} \frac{\|\nabla^{-1} \delta_t \bar{e}_\phi^{n+1}\|^2}{\tau_{n+1}} + \frac{1}{2} \|(\Delta + \beta) \bar{e}_\phi^{n+1}\|^2 + \frac{S}{2} \|\bar{e}_\phi^{n+1}\|^2 + |e_r^{n+1}|^2 \\
 &\lesssim \frac{\gamma_2^{\frac{3}{2}}}{2(1+\gamma_2)} \frac{\|\nabla^{-1} \bar{e}_\phi^1\|^2}{\tau_1} + \frac{1}{2} \|(\Delta + \beta) \bar{e}_\phi^1\|^2 + \frac{S}{2} \|\bar{e}_\phi^1\|^2 + |e_r^1|^2 \\
 &\quad + \sum_{k=1}^n \tau_{k+1} [|e_r^{n+1}|^2 + \|(\Delta + \beta) \bar{e}_\phi^n\|^2 + \|(\Delta + \beta) \bar{e}_\phi^{n-1}\|^2 + \|\bar{e}_\phi^n\|^2 \\
 &\quad + \|\bar{e}_\phi^{n-1}\|^2] + t_{n+1} [N^{-2m} \|\phi_t\|_{L^\infty(0,T;H^m)}^2 + N^{4-2m} \|\phi\|_{L^\infty(0,T;H^m)}^2] \\
 &\quad + \frac{\tau^2}{C_0} \int_{t_1}^{t_{n+1}} (\|\phi_t(s)\|_{H^1}^2 + \|\phi_{tt}(s)\|^2) ds + \tau^4 \int_0^{t_{n+1}} (\|\phi_{tt}(s)\|_{H^1}^2 + \|\phi_{ttt}(s)\|_{H^{-1}}^2) ds.
 \end{aligned} \tag{3.23}$$

We use the first order scheme (2.6) for the initial time step to get the following error equation for $n = 0$:

$$\begin{aligned}
& \left(\frac{\bar{e}_\phi^1}{\tau_1}, p_N \right) + (\nabla \bar{e}_\mu^1, \nabla p_N) = -(\tau_1^{-1} \int_0^{t_1} s \phi_{tt}(s) ds, p_N), \\
& (\bar{e}_\mu^1, q_N) = ((\Delta + \beta) \bar{e}_\phi^1, (\Delta + \beta) q_N) + S(\bar{e}_\phi^1, q_N) + \frac{e_r^1}{\sqrt{E_{1,N}^0 + C_0}} (F'(\phi_N^0), q_N) \\
& \quad + \left(\frac{r(t_1) F'(\phi_N^0)}{\sqrt{E_{1,N}^0 + C_0}} - \frac{r(t_1) F'(\phi_0(\mathbf{x}))}{\sqrt{E_1(\phi(t_1)) + C_0}}, q_N \right) - (F'(\phi_0(\mathbf{x})) - F'(\phi(t_1)), q_N), \\
& e_r^1 = \frac{\int_\Omega F'(\phi_N^0) \bar{e}_\phi^1 d\mathbf{x}}{2\sqrt{E_{1,N}^0 + C_0}} + \frac{1}{2} \int_\Omega \left[\frac{F'(\phi_N^0)}{\sqrt{E_{1,N}^0 + C_0}} - \frac{F'(\phi(t_1))}{\sqrt{E_1(\phi(t_1)) + C_0}} \right] \Pi_N(\phi(t_1) - \phi(t_0)) d\mathbf{x} \\
& \quad + \int_\Omega \frac{F'(\phi(t_1))}{\sqrt{E_1(\phi(t_1)) + C_0}} (\hat{e}_\phi^1 - \hat{e}_\phi^0) d\mathbf{x} - v_1^0 + v_2^0,
\end{aligned}$$

where $\phi_N^0 := \Pi_N \phi_0(\mathbf{x})$. Similar to the argument for the case $n \geq 1$, the following estimate can be easily derived with the assumption $\tau_1 \leq C\tau^{4/3}$

$$\begin{aligned}
& \frac{\|\nabla^{-1} \bar{e}_\phi^1\|^2}{2\tau_1} + \frac{1}{2} \|(\Delta + \beta) \bar{e}_\phi^1\|^2 + \frac{S}{2} \|\bar{e}_\phi^1\|^2 + |e_r^1|^2 \lesssim \tau_1^3 + \tau_1 N^{4-2m} \|\phi_0(\mathbf{x})\|_{H^m} \\
& \lesssim \tau^4 + \tau_1 N^{4-2m} \|\phi\|_{L^\infty(0,T;H^m)}.
\end{aligned} \tag{3.24}$$

Combining with (3.23), (3.24) and (3.3), together with the discrete Gronwall's lemma and the triangle inequality, the desired estimate (3.5) is obtained.

Next, we will prove the estimate (3.6), which can show that the numerical solution ϕ^n is of second-order accuracy in time with $C_0 \geq 1/\tau$. The error equation for $n \geq 1$ reads

$$\begin{aligned}
& (F_2^{n+1} \bar{e}_\phi, p_N) + (\nabla(\Delta + \beta) \bar{e}_\phi^{n+1}, \nabla(\Delta + \beta) p_N) + S(\nabla \bar{e}_\phi^{n+1}, \nabla p_N) \\
& = \left(1 - \frac{r^{n+1}}{\sqrt{E_{1,N}^n + C_0}} \right) (\nabla F'(\phi_N^{*,n+1}), \nabla p_N) - (\nabla(I_1^n + T_2^n), \nabla p_N) - (T_1^n, p_N).
\end{aligned}$$

Taking $p_N = (-\Delta)^{-1}(\delta_t \bar{e}_\phi^{n+1})$, and using the Young's inequality, we have

$$\begin{aligned}
& \frac{1}{2} \left[\left(\frac{\gamma_{n+2}^{\frac{3}{2}}}{1 + \gamma_{n+2}} + G(\gamma_*, \gamma_*) \right) \frac{\|\nabla^{-1} \delta_t \bar{e}_\phi^{n+1}\|^2}{\tau_{n+1}} - \frac{\gamma_{n+1}^{\frac{3}{2}}}{1 + \gamma_{n+1}} \frac{\|\nabla^{-1} \delta_t \bar{e}_\phi^n\|^2}{\tau_n} \right] \\
& + \frac{1}{2} [\|(\Delta + \beta) \bar{e}_\phi^{n+1}\|^2 - \|(\Delta + \beta) \bar{e}_\phi^n\|^2] + \frac{S}{2} [\|\bar{e}_\phi^{n+1}\|^2 - \|\bar{e}_\phi^n\|^2] \\
& \leq C(\gamma_*) \tau_{n+1} \left[\left| 1 - \frac{r^{n+1}}{\sqrt{E_{1,N}^n + C_0}} \right|^2 + \|\nabla I_1^n\|^2 + \|\nabla^{-1} T_1^n\|^2 + \|\nabla T_2^n\|^2 \right] \\
& + G(\gamma_*, \gamma_*) \frac{\|\nabla^{-1} \delta_t \bar{e}_\phi^{n+1}\|^2}{2\tau_{n+1}}.
\end{aligned} \tag{3.25}$$

Combined the estimate (3.18) for I_2^n with (3.5), it gives

$$\begin{aligned}
 & \left| 1 - \frac{r^{n+1}}{\sqrt{E_{1,N}^n + C_0}} \right|^2 \\
 &= \left| \frac{r^{n+1}}{\sqrt{E_{1,N}^n + C_0}} - \frac{r(t_{n+1})}{\sqrt{E_1(\phi(t_{n+1})) + C_0}} \right|^2 = \left| \frac{e_r^{n+1}}{\sqrt{E_{1,N}^n + C_0}} + r(t_{n+1}) \cdot I_2^n \right|^2 \\
 &\lesssim \frac{|e_r^{n+1}|^2}{C_0} + \frac{1}{C_0^2} \left(\tau_{n+1} \int_{t_n}^{t_{n+1}} \|\phi_t(s)\|^2 ds + \|\bar{e}_\phi^n\|^2 + N^{-2m} \|\phi\|_{L^\infty(0,T;H^m)} \right) \\
 &\lesssim \frac{\tau_0^2}{C_0^2} \int_0^T (\|\phi_t(s)\|_{H^1}^2 + \|\phi_{tt}(s)\|^2) ds + \frac{\tau^4}{C_0} \int_0^T (\|\phi_{tt}(s)\|_{H^1}^2 + \|\phi_{ttt}(s)\|_{H^{-1}}^2) ds \\
 &\quad + \frac{1}{C_0^2} \left(\tau_{n+1} \int_{t_n}^{t_{n+1}} \|\phi_t(s)\|^2 ds + \|\bar{e}_\phi^n\|^2 + N^{-2m} \|\phi\|_{L^\infty(0,T;H^m)} \right).
 \end{aligned} \tag{3.26}$$

Consequently, taking (3.26), the estimates of $\|I_1^n\|^2$, $\|T_1^n\|^2$ and $\|T_2^n\|^2$ into (3.25), summing it up from 1 to n, and applying the discrete Gronwall's lemma, we can deduce the desired estimate (3.6) and (3.7). Then the proof is completed. \square

Remark 3.1. Our error norms contain the terms $\|\nabla^{-1}e_\phi^1\|^2/\tau_1$ for $n = 0$ in (3.24) and $\|\nabla^{-1}\delta_t\bar{e}_\phi^{n+1}\|/\tau_{n+1}$ for $n \geq 1$ in (3.7). Thus, in order to guarantee the second order accuracy of the fully discrete scheme (2.15) with this type of error norm in (3.7), it is necessary to employ the first order scheme (2.6) with $\tau_1 \leq \tau^{4/3}$ to start the time marching. It is worth noting that the constant $C \exp(T)$ in the error estimates (3.5)-(3.7) would be rather large, which may be not optimal estimates particularly for the long-time simulation case. This exponential constant is commonly appeared in the error analysis for the time-stepping schemes using the discrete Gronwall's inequality as an analysis tool. To avoid using the discrete Gronwall's inequality, another possible way to establish the corresponding error estimates is to adopt the mathematical induction method. However, it is not easy to give a detailed uniform bound for the general positive constant C such as $C \leq 1$ in the derivation of the error estimate, which is a key issue in successfully deriving the error estimates by the mathematical induction approach. It is also an open, interesting problem now and needs more further effort.

4. NUMERICAL RESULTS

This section is devoted to numerically validating the theoretical results in terms of stability and accuracy. For simplicity, we set $\beta = 1, S = \varepsilon$, and the errors are computed by L^∞ -norm throughout the numerical tests.

4.1. Test of the convergence order. In this subsection, we investigate the accuracy of second order in time and spectral convergence in space for the fully discrete scheme (2.15). Here, we consider the PFC model with $\varepsilon = 0.025$ and the initial data, given by

$$\phi_0(x, y) = \sin\left(\frac{\pi x}{16}\right) \cos\left(\frac{\pi y}{16}\right).$$

The computational domain is set to be $(0, 32) \times (0, 32)$. At $T = 1$, a reference solution of the phase function ϕ^n is computed by the fully discrete scheme (2.15) with a fixed small uniform time step size $\Delta t = 1e - 5$ and a 256×256 space mesh. We first check the temporal accuracy

on the uniform temporal mesh. In Figure 1 (a), the temporal errors of the numerical solutions of the phase function ϕ^n with different time step sizes are plotted in log-log scale. It is shown that the scheme (2.15) with $C_0 = 1/\tau$ achieves the expected second order accuracy in time. We also display the second order approximation of the computed $r^{n+1}/\sqrt{E_{1,N}^n + C_0}$ to 1 in Figure 1 (b). Then we study the accuracy of the spatial discretization. In Figure 1 (c), we plot the L^∞ -errors in semi-log scale with respect to the Fourier mode number N . The error curve is almost a straight line in the semi-log scale, which indicates that the numerical solutions are exponentially convergent with respect to N . This is consistent with our theoretical results.

Next, we investigate the temporal error behaviors of the fully discrete scheme (2.15) on the nonuniform temporal mesh to validate our theoretical error estimates in Theorem 3.1. The nonuniform temporal mesh $\{\hat{t}_n\}_{n=0}^N$ used here is produced by 40% random perturbation of the uniform mesh $\{t_n = n\tau\}_{n=0}^N$, i.e., the random time grids are given by

$$\hat{t}_n := t_n + 0.4\tau \cdot \text{rand}(\cdot), \quad n = 0, 1, \dots, N,$$

where $\text{rand}(\cdot)$ is a random data from -1 to 1. The convergence order is computed by

$$\text{Order} = \frac{\log_{10}(\|e_\phi^M\|_\infty / \|e_\phi^{2M}\|_\infty)}{\log_{10}(\tau(M)/\tau(2M))},$$

where e_ϕ^M and $\tau(M)$ denote the L^∞ -norm error of ϕ at the final time T and the maximum time-step size for a total of M subintervals on $[0, T]$, respectively. In Table 1, we present convergence rates in time for the phase function ϕ^n in (2.15) at $T = 1$ with $\sigma = 1/2, 2/3$ and 1. It is observed the proposed scheme (2.15) achieves about second order accuracy for the phase function ϕ^n for all tested σ on the nonuniform mesh, even for the cases with the adjacent time step ratio $\gamma_n > 4.8645$. Thus it indicates that $\gamma_{**} = 4.8645$ may be not the optimal upper bound on the adjacent time step ratios, and deserves further investigation. In addition, compared to the numerical convergence results for the case of the uniform temporal meshes in Figure 1, the convergence order of the proposed scheme shown in Table 1 achieves obvious oscillations due to the randomness of the random nonuniform meshes used.

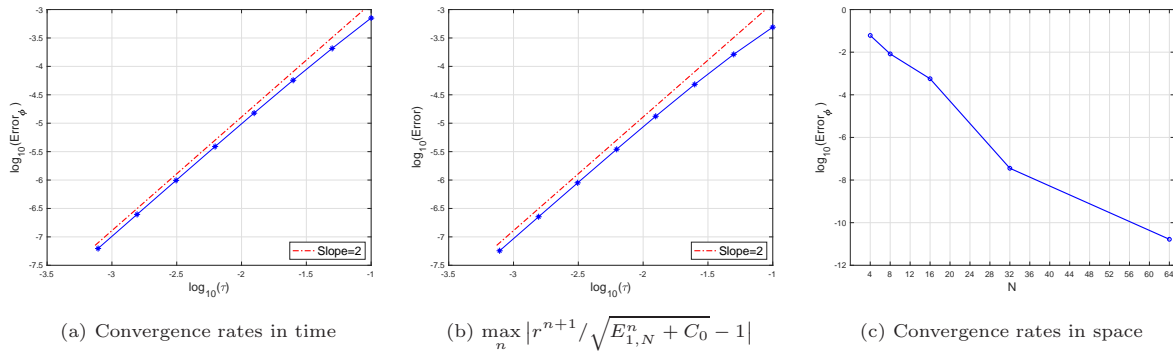


FIGURE 1. Convergence rates at $T = 1$ for the scheme (2.15) with $C_0 = 1/\tau$.

TABLE 1. Convergence rates in time at $T = 1$ for the phase function ϕ^n in (2.15) on nonuniform temporal meshes with $C_0 = 1/\tau$.

temporal mesh			$\sigma = \frac{1}{2}$		$\sigma = \frac{2}{3}$		$\sigma = 1$	
M	τ	$\max\{\gamma_n\}$	error	order	error	order	error	order
20	7.91e-2	3.64	8.30e-5	-	1.01e-4	-	1.45e-4	-
40	4.12e-2	4.79	1.42e-6	2.71	1.93e-5	2.55	2.95e-5	2.44
80	2.21e-2	4.16	4.49e-6	1.84	4.72e-6	2.26	6.11e-6	2.52
160	1.11e-2	5.41	7.53e-7	2.58	8.57e-7	2.47	1.28e-6	2.25
320	5.55e-3	6.40	8.55e-8	3.16	1.05e-7	3.00	1.52e-7	3.10
640	2.70e-3	5.24	2.18e-8	1.89	2.84e-8	1.81	4.09e-8	1.81
1280	1.39e-3	7.06	5.71e-9	2.03	7.12e-9	2.10	1.00e-8	2.12

4.2. Time adaptive strategy. In this part, the efficiency of the fully discrete scheme (2.15) with a time adaptive strategy is investigated through a long time phase transition process. As we know, the phase transition process usually goes through different stages, changing quickly at the beginning and then rather slowly afterwards, until it reaches a steady state after a long time evolution. Thus it would be very efficient to apply some time adaptive strategy in the simulation based on our proposed nonuniform BDF2 scheme (2.15).

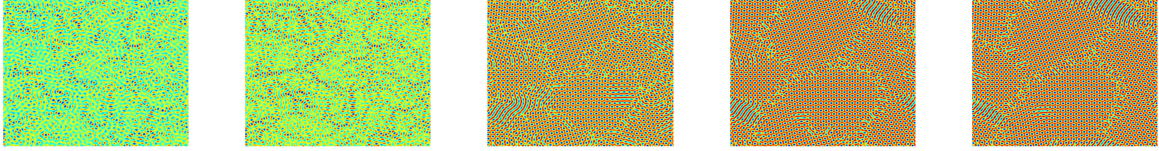
We consider the phase transition process governed by the PFC equation (1.2) with $\varepsilon = 0.1$ and the initial data $\phi_{i,j}^0 = 0.08 + \eta_{i,j}$, where $\eta_{i,j}$ is a random number between -0.08 and 0.08 . Here, the computational domain is set to be $\Omega = (0, 256)^2$. The time adaptive strategy proposed in [23] is adopted in the simulation with our fully discrete scheme (2.15):

$$\tau_{n+1} = \min \left(\max \left(\tau_{min}, \frac{\tau_{max}}{\sqrt{1 + \gamma |E'(t)|^2}} \right), 4.8645 \cdot \tau_n \right), \quad (4.1)$$

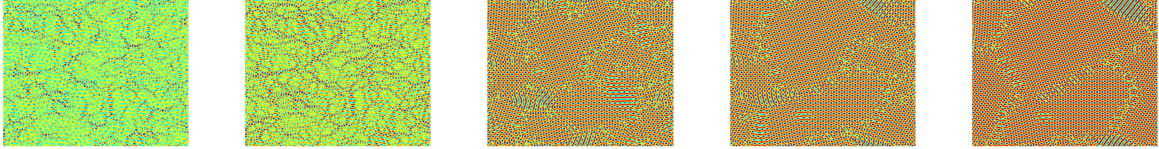
where τ_{min}, τ_{max} are predetermined minimum and maximum time step sizes, and γ is a positive constant. This type of the time adaptive strategy is based on the energy variation. It will automatically select small time steps when the energy decays rapidly and choose larger time steps otherwise. In this simulation, we set $\tau_{min} = 0.01$, $\tau_{max} = 5$ and $\gamma = 10^5$. Furthermore, 512×512 Fourier modes are used for the spatial discretization. In order to capture the characteristics of the phase transition process with rapid energy changes where the small time step size τ_{min} is used, we set $C_0 = 1/\tau_{min}$ to improve the local accuracy of our proposed numerical scheme at these times of rapid energy changes. It has also been checked that the chosen C_0 is large enough such that $E_1(\cdot) + C_0 > 0$.

In Figure 2, we plot the evolutions of the phase function ϕ^n up to $T = 5000$ with four different types of temporal meshes, viz., the fixed large time step mesh with $\tau = 5$, two different ones from the time adaptive strategy (4.1), and the uniform small time step mesh with $\tau = 0.01$. In Figure 3 (a), it shows that there is no obvious difference at $t = 20$, and the corresponding energies consist with each other at this stage. After the energy goes through a large variation stage, the fixed large time step with $\tau = 5$ yields inaccurate numerical solutions, while both two tested adaptive time strategies with $\tau_{max} = 1$ and 5 give correct phase transition patterns consistent with the results obtained by the small time step case $\tau = 0.01$. It is observed in Figure 3 (a) and (b) that both the computed modified energy \tilde{E}_N^n and the computed original energy $E(\phi_N^n)$ are dissipative

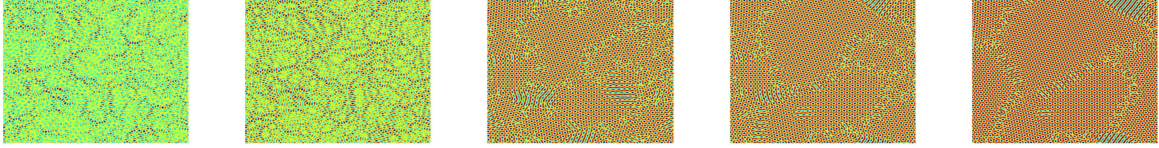
in time for the tested four different types of temporal meshes. Moreover, as shown in Figure 3 (b), the energy dissipation of the proposed scheme (2.15) with the adaptive strategy (4.1) consists very well with the one using the fixed small time step $\tau = 0.01$. The corresponding time step sizes are also plotted in Figure 3 (c), which shows the efficiency of our proposed scheme (2.15) with the adaptive strategy (4.1) during this long time simulation. Furthermore, using a smaller τ_{max} in adaptive time strategy (4.1) certainly improves the accuracy more or less, but may lead to considerable increase in the computational cost, as shown in Figure 3 (c).



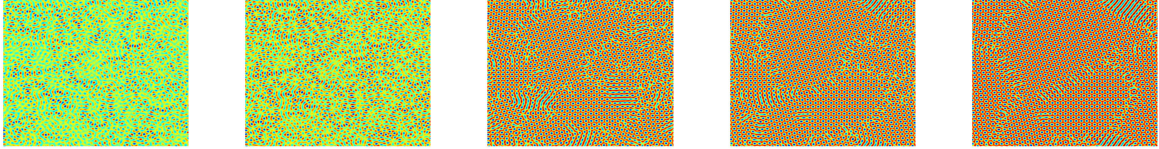
(a) solutions with fixed large time step size $\tau = 5$.



(b) solutions with adaptive time steps with $\tau_{min} = 0.01, \tau_{max} = 5$ and $\gamma = 10^5$.



(c) solutions with adaptive time steps with $\tau_{min} = 0.01, \tau_{max} = 1$ and $\gamma = 10^5$.



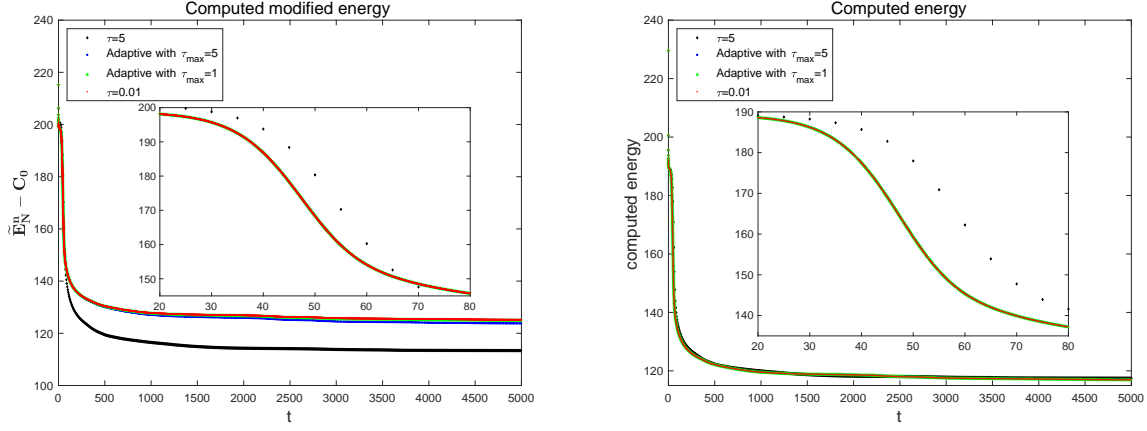
(d) solutions with fixed small time step size $\tau = 0.01$.

FIGURE 2. Solution snapshots of the phase transition process for the PFC equation at around $t = 20, 50, 500, 1500$, and 5000 , respectively.

4.3. Crystal growth in a supercooled liquid. In this subsection, we simulate the growth of a polycrystal in a supercooled liquid. Initially, three crystallites with different orientations are given by

$$\phi_0(x_l, y_l) = 0.285 + 0.446 \left(\cos \left(\frac{0.66}{\sqrt{3}} y_l \right) \cos(0.66 x_l) - 0.5 \cos \left(\frac{1.32}{\sqrt{3}} y_l \right) \right), \quad l = 1, 2, 3,$$

where x_l and y_l define a local system of cartesian coordinates that is oriented with the crystallite lattice. Similar numerical examples can be found in [6, 9, 16, 20, 31]. The computed domain is


 (a) the computed modified energy $\tilde{E}_N^n - C_0$

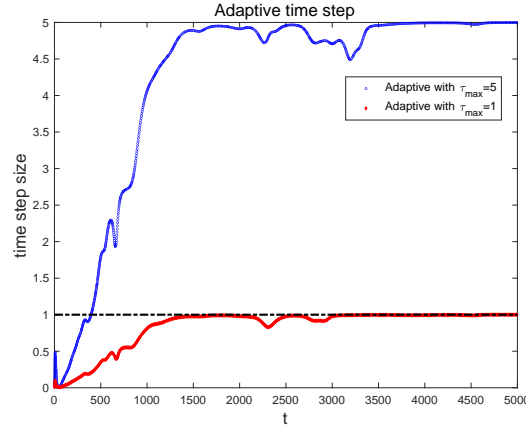
 (b) the computed energy $E(\phi^n)$

 (c) adaptive time step sizes with $\tau_{max} = 1$ and $\tau_{max} = 5$

FIGURE 3. Evolution in time of the modified energy, the original energy, and the adaptive time step sizes.

$(0, 800)^2$, $\varepsilon = 0.25$, and the initial three crystallites are located in the blocks with length of 40 in the computed domain, seeing Figure 4 for the case of $t = 0$. In order to obtain three different orientations of the crystallites, we define the local coordinates (x_l, y_l) by using the following affine transformation of the global coordinates (x, y) ,

$$\begin{cases} x_l = x \cos(\theta) - y \sin(\theta), \\ y_l = x \sin(\theta) + y \cos(\theta), \end{cases}$$

where $\theta = -\pi/4, 0, \pi/4$ for $l = 1, 2, 3$, respectively. This produces a rotation given by the angle θ .

The simulation is performed by the second order scheme (2.15) with $\sigma = 1$ and 1024×1024 Fourier modes. Here, we use two types of temporal meshes: the fixed small time step with $\tau = 0.01$ and the adaptive strategy (4.1) with $\tau_{min} = 0.01, \tau_{max} = 1$ and $\gamma = 10$. In Figure 4, we display the evolution of the crystal growth up to $T = 1500$ for these two types of temporal

meshes, respectively. It is observed that the snapshots of the crystal growth consist with each other at same time stages for these two temporal meshes. The growth of the crystalline phase and the motion of well-defined crystal–liquid interfaces are observed. Moreover, it shows that the different alignment of the crystallites causes defects and dislocations. This phenomenon has been also observed in [6, 9, 16, 20, 31]. In Figure 5, the evolution of the modified energy, the original energy, and the corresponding adaptive time step sizes are plotted to validate the stability and the efficiency of our proposed scheme (2.15) with the adaptive strategy (4.1).

Remark 4.1. *As shown in Figure 3 and Figure 5, the evolutions of the computed original energy with the tested time adaptive strategies are in agreement with the one computed by the small time step $\tau = 0.01$ better than the case of the computed modified energy. This may be due to the computed auxiliary variable r^n and the extra term $\frac{(2\sigma-1)\gamma_{n+1}^{3/2}}{2+2\gamma_{n+1}} \frac{\|\nabla^{-1}(\phi_N^n - \phi_N^{n-1})\|^2}{\tau_n}$ contained in the modified energy in (2.16).*

5. CONCLUDING REMARKS

We have developed and analyzed a linear second order nonuniform BDF scheme based on the SAV approach for the PFC model. The energy stability of the proposed scheme is established for the nonuniform temporal mesh with a mild restriction on the adjacent time step ratio $\gamma_n \leq 4.8645$. Although we only use a first order method to approximate the auxiliary variable $r(t)$, the second order accuracy of the phase function ϕ^n can be guaranteed by setting a large enough positive constant C_0 such that $C_0 \geq 1/\tau$. Moreover, a rigorous error estimate of our proposed fully discrete nonuniform BDF2 scheme is established with some proper assumptions on the regularity of the solution. Finally, a series of numerical tests have been carried out to validate the theoretical results and the efficiency of the proposed scheme combined with the time adaptive strategy.

REFERENCES

- [1] A. Baskaran, J. S. Lowengrub, C. Wang, and S. M. Wise. Convergence analysis of a second order convex splitting scheme for the modified phase field crystal equation. *SIAM J. Numer. Anal.*, 51(5):2851–2873, 2013.
- [2] W. Chen, X. Wang, Y. Yan, and Z. Zhang. A second order BDF numerical scheme with variable steps for the Cahn–Hilliard equation. *SIAM J. Numer. Anal.*, 57(1):495–525, 2019.
- [3] L. Dong, W. Feng, C. Wang, S. M. Wise, and Z. Zhang. Convergence analysis and numerical implementation of a second order numerical scheme for the three-dimensional phase field crystal equation. *Comput. Math. Appl.*, 75(6):1912–1928, 2018.
- [4] Q. Du, L. Ju, X. Li, and Z. Qiao. Maximum bound principles for a class of semilinear parabolic equations and exponential time differencing schemes. *SIAM Rev.*, 63(2):317–359, 2021.
- [5] K. R. Elder and M. Grant. Modeling elastic and plastic deformations in nonequilibrium processing using phase field crystals. *Phys. Rev. E*, 70(5):051605, 2004.
- [6] K. R. Elder, M. Katakowski, M. Haataja, and M. Grant. Modeling elasticity in crystal growth. *Phys. Rev. Lett.*, 88(24):245701, 2002.
- [7] C. M. Elliott and A. M. Stuart. The global dynamics of discrete semilinear parabolic equations. *SIAM J. Numer. Anal.*, 30(6):1622–1663, 1993.
- [8] D. J. Eyre. Unconditionally Gradient Stable Time Marching the Cahn–Hilliard Equation. *Mater. Res. Soc. Sympos. Proc.*, 529:39–46, 1998.
- [9] H. Gomez and X. Nogueira. An unconditionally energy-stable method for the phase field crystal equation. *Comput. Methods Appl. Mech. Eng.*, 249-252:52–61, 2012.

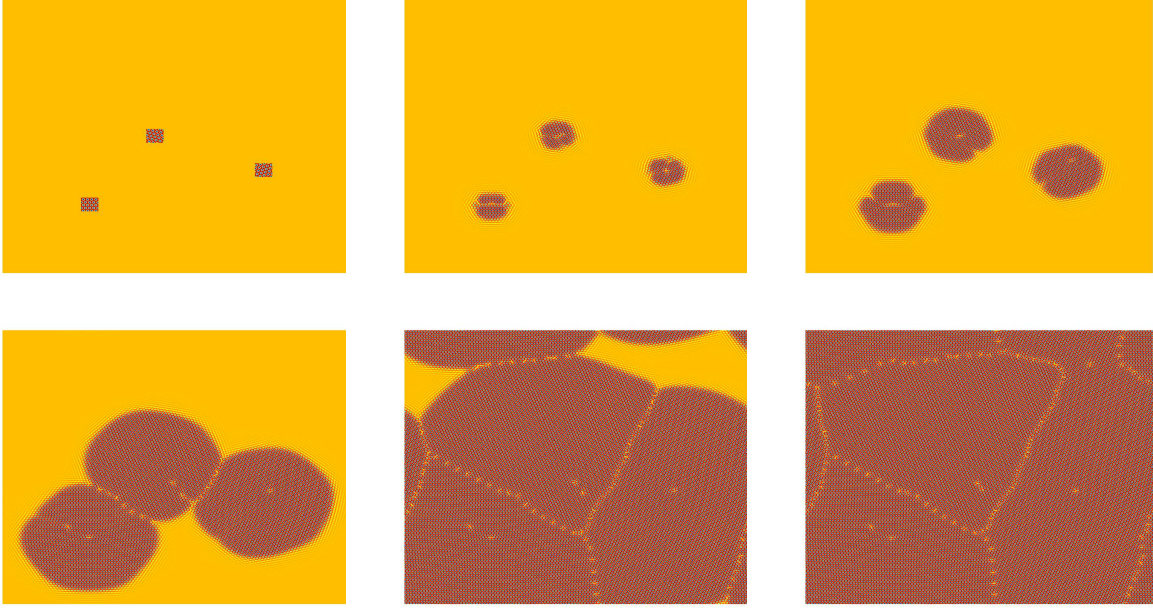
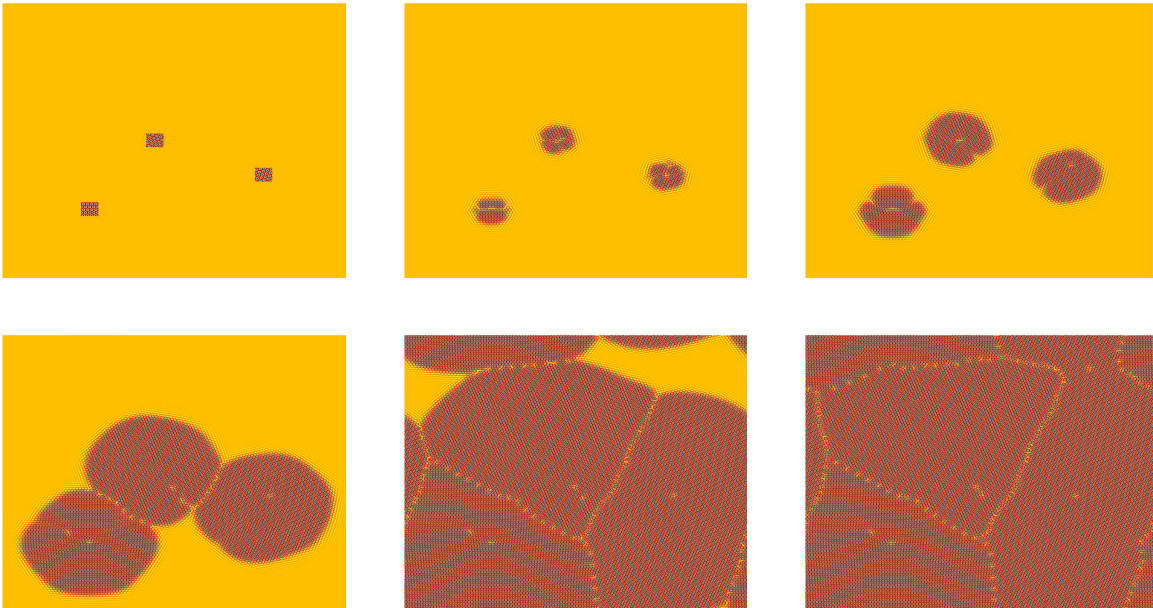

 (a) Solutions with fixed time step size $\tau = 0.01$

 (b) Solutions with adaptive time steps with $\tau_{min} = 0.01$, $\tau_{max} = 1$ and $\gamma = 10$.

 FIGURE 4. Solution snapshots of crystal growth for the PFC equation at around $t = 0, 100, 200, 400, 800$ and 1500 , respectively.

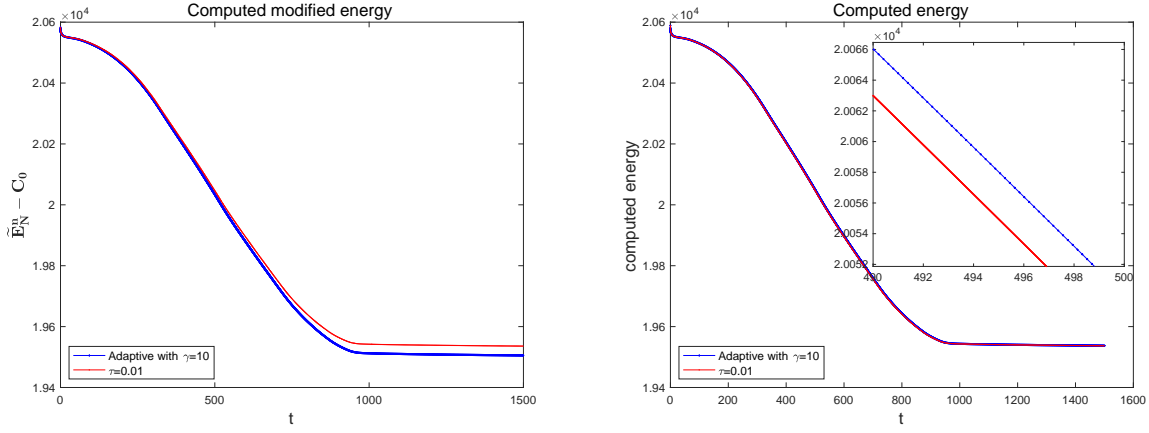
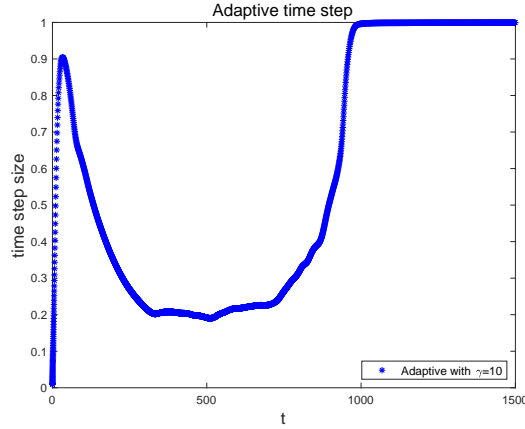
(a) the computed modified energy $\tilde{E}_N^n - C_0$ (b) the computed energy $E(\phi^n)$ (c) adaptive time step sizes with $\gamma = 10$

FIGURE 5. Evolution in time of the energy and the adaptive time step size for crystal growth.

- [10] Z. Guan, J. S. Lowengrub, C. Wang, and S. M. Wise. Second order convex splitting schemes for periodic nonlocal Cahn-Hilliard and Allen-Cahn equations. *J. Comput. Phys.*, 277:48–71, 2014.
- [11] R. Guo and Y. Xu. Local discontinuous galerkin method and high order semi-implicit scheme for the phase field crystal equation. *SIAM J. Sci. Comput.*, 38(1):A105–A127, 2016.
- [12] D. Hou, M. Azaiez, and C. Xu. A variant of scalar auxiliary variable approaches for gradient flows. *J. Comput. Phys.*, 395:307–332, 2019.
- [13] D. Hou and Z. Qiao. An implicit–explicit second–order BDF numerical scheme with variable steps for gradient flows. *J. Sci. Comput.*, 94(2):39, 2023.
- [14] D. Hou and C. Xu. Robust and stable schemes for time fractional molecular beam epitaxial growth model using SAV approach. *J. Comput. Phys.*, 445(15):110628, 2021.
- [15] D. Hou and C. Xu. A second order energy dissipative schemes for time fractional L^2 gradient flows using SAV approach. *J. Sci. Comput.*, 90:25, 2022.
- [16] Z. Hu, S. M. Wise, C. Wang, and J. S. Lowengrub. Stable and efficient finite-difference nonlinear-multigrid schemes for the phase field crystal equation. *J. Comput. Phys.*, 228(15):5323–5339, 2009.
- [17] L. Ju, X. Li, and Z. Qiao. Generalized SAV–exponential integrator schemes for Allen–Cahn type gradient flows. *SIAM J. Numer. Anal.*, 60(4):1905–1931, 2022.

- [18] L. Ju, X. Li, and Z. Qiao. Stabilized exponential–SAV schemes preserving energy dissipation law and maximum bound principle for the Allen–Cahn type equations. *J. Sci. Comput.*, 92(2):66, 2022.
- [19] Q. Li, L. Mei, and B. You. A second-order, uniquely solvable, energy stable BDF numerical scheme for the phase field crystal model. *Appl. Numer. Math.*, 134:46–65, 2018.
- [20] X. Li and J. Shen. Stability and error estimates of the SAV Fourier-spectral method for the phase field crystal equation. *Adv. Comput. Math.*, 46:48, 2020.
- [21] H. Liao, B. Ji, and L. Zhang. An adaptive BDF2 implicit time-stepping method for the phase field crystal model. *IMA J. Numer. Anal.*, 42(1):649–679, 2022.
- [22] Z. Liu and X. Li. The fast scalar auxiliary variable approach with unconditional energy stability for nonlocal Cahn–Hilliard equation. *Numer. Methods Partial Differ. Equ.*, 37(1):244–261, 2021.
- [23] Z. Qiao, Z. Zhang, and T. Tang. An adaptive time-stepping strategy for the molecular beam epitaxy models. *SIAM J. Sci. Comput.*, 33(3):1395–1414, 2011.
- [24] J. Shen, T. Tang, and L. L. Wang. *Spectral methods, Algorithms, Analysis and Applications*. Springer, Berlin, 2010.
- [25] J. Shen and J. Xu. Convergence and error analysis for the scalar auxiliary variable(SAV) schemes to gradient flows. *SIAM J. Numer. Anal.*, 56(5):2895–2912, 2018.
- [26] J. Shen, J. Xu, and J. Yang. The scalar auxiliary variable (SAV) approach for gradient flows. *J. Comput. Phys.*, 353:407–416, 2018.
- [27] J. Shen, J. Xu, and J. Yang. A new class of efficient and robust energy stable schemes for gradient flows. *SIAM Rev.*, 61(3):474–506, 2019.
- [28] C. Wang and S. M. Wise. An energy stable and convergent finite–difference scheme for the modified phase field crystal equation. *SIAM J. Numer. Anal.*, 49(3):945–969, 2011.
- [29] S. M. Wise, C. Wang, and J. S. Lowengrub. An energy-stable and convergence finite–difference scheme for the phase field crystal equation. *SIAM J. Numer. Anal.*, 47(1):2269–2288, 2009.
- [30] X. Yang. Linear, first and second-order, unconditionally energy stable numerical schemes for the phase field model of homopolymer blends. *J. Comput. Phys.*, 327:294–316, 2016.
- [31] X. Yang and D. Han. Linearly first- and second-order, unconditionally energy stable schemes for the phase field crystal model. *J. Comput. Phys.*, 88(330):1116–1134, 2017.
- [32] Z. Yang, L. Lin, and S. Dong. A family of second-order energy-stable schemes for Cahn–Hilliard type equations. *J. Comput. Phys.*, 383:24–54, 2019.
- [33] Z. Zhang, Y. Ma, and Z. Qiao. An adaptive time-stepping strategy for solving the phase field crystal model. *J. Comput. Phys.*, 249:204–215, 2013.
- [34] J. Zhao, Q. Wang, and X. Yang. Numerical approximations for a phase field dendritic crystal growth model based on the invariant energy quadratization approach. *Int. J. Numer. Meth. Eng.*, 110(3):279–300, 2017.